Journal of Marine Science and Application (2023) 22: 247-259
https://doi.org/10.1007/s11804-023-00328-8

RESEARCH ARTICLE

Effects of Material Characteristics on Nonlinear Dynamics of Viscoelastic Axially Functionally Graded Material Pipe Conveying Pulsating Fluid

Guangming Fu[1], Yuhang Tuo[1,2], Heen Zhang[3], Jian Su[4], Baojiang Sun[1], Kai Wang[1] and Min Lou[1]

Received: 30 May 2022 / Accepted: 13 July 2022

Abstract

The nonlinear dynamic behaviors of viscoelastic axially functionally graded material (AFG) pipes conveying pulsating internal flow are very complex. And the dynamic behavior will induce the failure of the pipes, and research of vibration and stability of pipes becomes a major concern. Considering that the elastic modulus, density, and coefficient of viscoelastic damping of the pipe material vary along the axial direction, the transverse vibration equation of the viscoelastic AFG pipe conveying pulsating fluid is established based on the Euler-Bernoulli beam theory. The generalized integral transform technique (GITT) is used to transform the governing fourth-order partial differential equation into a nonlinear system of fourth-order ordinary differential equations in time. The time domain diagram, phase portraits, Poincaré map and power spectra diagram at different dimensionless pulsation frequencies, are discussed in detail, showing the characteristics of chaotic, periodic, and quasi-periodic motion. The results show that the distributions of the elastic modulus, density, and coefficient of viscoelastic damping have significant effects on the nonlinear dynamic behavior of the viscoelastic AFG pipes. With the increase of the material property coefficient k, the transition between chaotic, periodic, and quasi-periodic motion occurs, especially in the high-frequency region of the flow pulsation.

Keywords Axially functionally graded pipe; Pipe conveying pulsating flow; Integral transforms; Nonlinear dynamics; Chaotic motion; Quasi-periodic motion

Article Highlights

- The transverse vibration equation is established for the viscoelastic axially functionally graded material (AFG) pipe conveying pulsating fluid;
- The generalized integral transform technique is developed to analyze the nonlinear dynamics of AFG pipes;
- The effects of the elastic modulus, density, and coefficient of viscoelastic damping on nonlinear dynamics of AFG pipes are discussed.

✉ Guangming Fu
fu@upc.edu.cn

[1] Key Laboratory of Unconventional Oil & Gas Development (China University of Petroleum (East China)), Ministry of Education, Qingdao 266580, China

[2] China Petroleum Pipeline Engineering Co., Ltd., Langfang 065201, China

[3] CNPC Offshore Engineering Company Limited, Beijing 100028, China

[4] Nuclear Engineering Department, COPPE, Federal University of Rio de Janeiro, Rio de Janeiro 21941-972, Brazil

1 Introduction

Pipe conveying fluid is an important structure in a number of engineering fields, and is widely used in heat exchangers, nuclear industry, petroleum transportation, aviation and other industries. Due to the excitation of the external and internal fluids, pipe structural properties, and other factors, pipes conveying fluid will have complex dynamic behaviors (Jin,1997; Jin and Song, 2005; Wang and Chen, 2019). The vibration and stability of pipes becomes a major concern over the past decades. Paidoussis and collaborators (Paidoussis and Moon, 1988; Paidoussis et al., 1989; Paidoussis et al., 1992; Paidoussis and Semler, 1993) investigated the nonlinear dynamic behavior of cantilever pipes through experiments and numerical simulations, the chaotic motion behavior through phase portraits, bifurcation diagrams and Poincaré maps, and found that chaos occurred through period-doubling bifurcation. Tang and Dowell (1988) studied the chaotic phenomenon of cantilevered pipes using experimental method and numerical technique,

and the results showed that chaotic motion would occur when the flow rate exceeded a critical value. The nonlinear dynamic behavior of pipe conveying pulsating fluid with high average velocity and spring constraint were investigated by Wang and his collaborators (Wang, 2009; Wang et al., 2017), and they found that the average velocity and spring constraints have significant effects on the nonlinear dynamic response of the system. Ni et al. (2014) studied the nonlinear dynamic behavior of two coupled pipe system conveying pulsating fluids, and the results showed that the connection stiffness had a significant effect on the dynamics of the coupled pipe system. For some parameters, the motion types of the two pipes may be out of synchronization. Oyelade and Oyediran (2020) studied the nonlinear dynamics of pipes under thermal loads, and effects of the initial curvature, temperature, axial force, pressure, longitudinal and transverse strain were took into account. The nonlinear analysis results showed that the amplitude of pipe motion was significantly increased due to the influence of thermal load.

Functional gradient materials (FGM) are new heterogeneous composite materials made of two or more homogeneous materials, and it has been widely used in various fields due to their excellent properties. By varying the volume fraction of each homogeneous material, the properties of AFG pipes vary continuously along the pipe from one end to the other. Comparing with the traditional composite pipe (Nikbakht et al., 2019; Wang and Soares, 2021; Fu et al., 2022a; Fu et al., 2022b; Wang et al., 2022), the AFG pipe can eliminate the interface effects of traditional uniform composites. For instance, the AFG pipe can be used in optimized design of control lines in subsea engineering and aerospace engineering by varying the properties along the axial direction (Gupta and Talha, 2015). The dynamic behaviour of functionally gradient pipes become a major concern over the past decade. However, most of the literature mainly focuses on the linear dynamics behavior of the AFG pipes. An and Su (2017) studied the linear vibration characteristics of AFG pipes with simple support, and analyzed the influence of the material elastic modulus, density distribution and flow rate on the free vibration characteristics of AFG pipes. Zhou et al. (2018) discussed the linear dynamics of cantilever AFG pipes, and analyzed the influence of the elastic modulus and density distribution on the critical flow rate. Heshmati (2020) analyzed the influence of different eccentricity and power rate exponents on the critical flow rate of the radially functional gradient material pipes with eccentric defects. Deng et al. (2017) studied the dynamic characteristics of multi-span viscoelastic FGM pipes by the dynamic stiffness method, and analyzed the influence of the volume fraction index, flow velocity, internal pressure and damping on pipe stability and frequency effects. Recently, there are few studies discussing the nonlinear dynamics of FGM pipes. Lu et al. (2020) studied the fatigue life of AFG pipes under the conditions of primary resonance and 1:3 internal resonance. Tang and Yang (2018) applied the homotopy analysis method to study the post-buckling behavior and nonlinear vibration characteristics of radially functional gradient pipes with steady internal flow. The results showed that the statics and dynamics of pipe can be significantly changed by the material properties. Khodabakhsh et al. (2020) used the Timoshenko beam model to study the post-buckling behavior and nonlinear vibration characteristics of radially FGM pipes considering shear deformation and moment of inertia, and discussed the effects of moment of inertia and shear deformation on buckling behavior, critical flow rate, nonlinear frequency and dimensionless amplitude. Shafiei and She (2018) predicted the vibration characteristics of a two-dimensional FGM based on the higher-order theory. The generalized differential quadrature method (GDQM) was employed in his studies, and the influences of non-local parameters, strain gradient parameters, temperature and material variations on the vibration characteristics of FGM pipes under different boundary conditions are discussed. Ebrahimi-Mamaghani et al. (2020) investigated the thermo-mechanical vibration of AFG pipe conveying fluid. Using Rayleigh beam theory and considering the linear and nonlinear stress-temperature relationship, the govern equation of the system was estabulished. The effects of the material gradient, power index, boundary conditions, moment inertia factor, temperature and boundary conditions on the dynamic structure of the system are discussed. Dai et al. (2019) investigated the thermoelastic vibration of AFG pipe conveying fluid considering temperature variation effects. The differential quadrature method was employed to solve the govern equations based on Euler-Bernoulli beam theory. The influence of the elasticity and thermoelasticity gradients on the material performance were discussed. Most recently, Tuo et al. (2022) investigated the linear stability of axially functionally graded pipe conveying fluid using the generalized integral transform technique (GITT) for four combinations of boundary conditions, and the results showed that the complex frequency, critical velocity of buckling instability and coupled flutter of the axially functionally graded pipe are significantly influenced by the elastic modulus gradient.

The present work aims to investigate the nonlinear dynamic behavior of AFG pipe conveying pulsating fluid. Based on the Euler-Bernoulli beam theory, the nonlinear vibration equation of an AFG pipe conveying pulsating flow with simply supported boundary condition was estabulished. Using the GITT technique (Cotta et al., 2019; Fu et al., 2019; Li et al., 2020; Tuo et al., 2022; Fu et al., 2022c), the governing nonlinear partial differential equations were transformed into a nonlinear system of coupled ordinary differential equations, which were solved numerically using the build-in function *NDsolve* of the software

Mathematica. Furthermore, the GITT technique intrinsically keeps the property of the partial differential equations according to eigenvalues, which is different from the way adding auxiliary variable to construct the physical-preserving scheme (Zhao et al., 2017; Shen et al., 2018; Jiang et al., 2022, 2023). With this model, The effects of elastic modulus, density and viscoelastic damping coefficient in the axial direction on the nonlinear dynamic behavior were studied. The bifurcation, phase portrait, and energy spectra diagrams were obtained to investigate the nonlinear dynamic behavior characteristics of the AFG pipe.

2 Theoretical model

Considering a viscoelastic AFG pipe conveying a pulsating fluid, as illustrated in Figure 1. The pipe has a length L, inner radius r_o, outer radius r_1, and cross-sectional area A_p. The fluid has a mass per unit length m_f and an average velocity $u(t)$. The elastic modulus $E(x)$, coefficient of viscoelastic damping $E^*(x)$, and density of the AFG pipe are given by Shariati et al. (2020), Loghman et al. (2021), and Babilio (2014) :

$$E(x) = E_0 f(x) \tag{1a}$$

$$E^*(x) = E_0^* f(x) \tag{1b}$$

$$\rho(x) = \rho_0 g(x) \tag{1c}$$

$$f(x) = 1 + (\alpha_E - 1)\left(\frac{x}{L}\right)^k \tag{2a}$$

$$h(x) = 1 + (\alpha_{E^*} - 1)\left(\frac{x}{L}\right)^k \tag{2b}$$

$$g(x) = 1 + (\alpha_\rho - 1)\left(\frac{x}{L}\right)^k \tag{2c}$$

Figure 1 Schematic of an axially functionally graded material pipe

where $\alpha_E = E_L/E_O$ is the elastic modulus ratio, $\alpha_{E^*} = E_L^*/E_O^*$ the coefficient of the viscoelastic damping ratio, and $\alpha_\rho = \rho_L/\rho_O$ the density ratio. E_1, E_1^*, ρ_1 and E_O, E_O^* and ρ_O represent the elastic modulus, coefficient of viscoelastic damping and density at the left and right ends of the pipe, respectively. Figure 2 shows the variation of the material properties along the axial under different exponents k when α_E=2.

The stress-strain relationship of the Kelvin-Voigt type of viscoelastic material is given by:

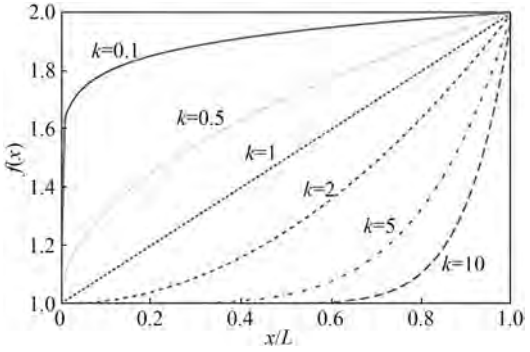

Figure 2 Variation of the material properties along the axial under different exponents k (α_E=2)

$$\sigma = \left(E(x) + E^*(x)\frac{\partial}{\partial t}\right)\varepsilon \tag{3}$$

Bending moment is expressed as:

$$M = \left(E(x) + E^*(x)\frac{\partial}{\partial t}\right) I \frac{\partial^2 w}{\partial x^2} \tag{4}$$

where $w(x,t)$ is the transversal deflection of the pipe.

Shear force is given by:

$$S = -\frac{\partial M}{\partial x} = -\frac{\partial}{\partial x}\left[\left(E(x) + E^*(x)\frac{\partial}{\partial t}\right) I \frac{\partial^2 w}{\partial x^2}\right] \tag{5}$$

The lateral vibration equation of an AFG pipe is written as (Paidoussis and Issid,1974; Paidoussis,1987; Paidoussis and Li,1993),

$$-\frac{\partial^2}{\partial x^2}\left[\left(E(x) + E^*(x)\frac{\partial}{\partial t}\right) I \frac{\partial^2 w}{\partial x^2}\right] + \frac{\partial}{\partial x}\left[\left(T - A_f p_1\right)\frac{\partial w}{\partial x}\right] = m_f\left(\frac{\partial^2 w}{\partial t^2} + 2u\frac{\partial^2 w}{\partial x \partial t} + u^2\frac{\partial^2 w}{\partial x^2} + \frac{\mathrm{d}u}{\mathrm{d}t}\frac{\partial w}{\partial x}\right) + m_f(x)\frac{\partial^2 w}{\partial t^2} \tag{6}$$

where, T is the axial force, A_f is the cross-sectional flow area and p_1 is the fluid pressure.

Considering that the extension of the pipe due to bending deformation will produce additional axial force:

$$T - A_f p_1 = T_0 - A_f p_o(1 - 2\nu\delta) + m_f\frac{\mathrm{d}u}{\mathrm{d}t}(x - L) + \left[E(x) + E^*(x)\frac{\partial}{\partial t}\right]\frac{A_p}{2L}\int_0^L\left(\frac{\partial w}{\partial x}\right)^2 \mathrm{d}x \tag{7}$$

where, T_0 is static tension, and p_0 is the pressure of internal flow at $x = L$.

Substituting Eq-7 into the lateral vibration equation (Eq-6) of the AFG pipe, we have:

$$\frac{\partial^2}{\partial x^2}\left[E(x)I\frac{\partial^2 w}{\partial x^2}+E^*(x)I\frac{\partial^3 w}{\partial x^2\partial t}\right]+\left[m_f u^2-T_0+A_f p_0(1-2v\delta)+m_f\frac{\mathrm{d}u}{\mathrm{d}t}(L-x)\right]\frac{\partial^2 w}{\partial x^2}-\frac{\partial}{\partial x}\left[\left(E(x)+E^*(x)\frac{\partial}{\partial t}\right)\frac{A_p}{2L}\int_0^L\left(\frac{\partial w}{\partial x}\right)^2\mathrm{d}x\frac{\partial w}{\partial x}\right]+2m_f u\frac{\partial^2 w}{\partial x\partial t}+\left[m_f+\rho(x)A_p\right]\frac{\partial^2 w}{\partial t^2}=0 \tag{8}$$

Neglecting the pressure p_0 and static tension T_0, we have:

$$\frac{\partial^2}{\partial x^2}\left[E(x)I\frac{\partial^2 w}{\partial x^2}+E^*(x)I\frac{\partial^3 w}{\partial x^2\partial t}\right]+\left[m_f u^2+m_f\frac{\mathrm{d}u}{\mathrm{d}t}(L-x)\right]\frac{\partial^2 w}{\partial x^2}-\frac{\partial}{\partial x}\left[\left(E(x)+E^*(x)\frac{\partial}{\partial t}\right)\frac{A_p}{2L}\int_0^L\left(\frac{\partial w}{\partial x}\right)^2\mathrm{d}x\frac{\partial w}{\partial x}\right]+2m_f u\frac{\partial^2 w}{\partial x\partial t}+\left[m_f+\rho(x)A_p\right]\frac{\partial^2 w}{\partial t^2}=0 \tag{9}$$

The following dimensionless parameters are introduced:

$$\xi=\frac{x}{L},w^*=\frac{w}{L},\tau=\left(\frac{E_oI}{m_f+\rho_oA_p}\right)^{1/2}\frac{t}{L^2},\quad \alpha_0=\frac{E_0^*}{L^2}\sqrt{\frac{I}{E_0(m_f+\rho_0A_p)}},\quad Q=\frac{A_pL^2}{2I},\beta=\frac{m_f}{m_f+\rho_oA_p},\quad \alpha(\xi)=\frac{\rho(x)A_p}{m_f+\rho_oA_p},U=uL\left(\frac{m_f}{E_oI}\right)^{1/2} \tag{10}$$

The dimensionless governing equation is then obtained as (dropping the asterisks of w^* for simplicity):

$$f(\xi)w''''+2f'(\xi)w'''+\left[f''(\xi)+U^2+\sqrt{\beta}\dot{U}(1-\xi)\right]w''+\alpha_o h''(\xi)\dot{w}''+2\alpha_o h'(\xi)\dot{w}'''+\alpha_o h(\xi)\dot{w}''''-Q\left[f(\xi)w''+f'(\xi)w'\right]\int_0^1(w')^2\mathrm{d}\xi+2\sqrt{\beta}U\dot{w}'-2\alpha_o Q\left[h(\xi)w''+h'(\xi)w'\right]\int_0^1 w'\dot{w}'\mathrm{d}\xi+\left[\alpha(\xi)+\beta\right]\ddot{w}=0 \tag{11}$$

Here, the prime "′" denotes the spatial derivative in ξ and the dot "·" denotes the time derivative in τ.

The internal fluid velocity of the AFG pipe is assumed to be sinusoidal and given in the following dimensionless form:

$$U=U_0(1+\psi\sin(\omega\tau)) \tag{12}$$

where U_0 is the average flow velocity, ψ is the pulsation amplitude, and ω is the dimensionless pulsation frequency.

The boundary conditions for simply-supported ends are:

$$w(0,\tau)=w(1,\tau)=w''(0,\tau)=w''(1,\tau)=0 \tag{13}$$

3 Integral transform solution

Following the formalism of the generalized integral transform technique, the governing equation of the following auxiliary eigenvalue problem is employed (Cotta et al., 2019; Fu et al., 2019; Li et al., 2020) :

$$\frac{\mathrm{d}^4X_i(\xi)}{\mathrm{d}\xi^4}=\mu_i^4X_i(\xi),\ 0<\xi<1 \tag{14}$$

with simply supported (SS) boundary conditions:

$$X_i(0)=X_i''(0)=X_i(1)=X_i''(1)=0 \tag{15}$$

where the eigenfunctions $X_i(\xi)$ and eigenvalues μ_i are given by:

$$X_i(\xi)=\sqrt{2}\sin(\mu_i\xi),\ i=1,2,3\cdots \tag{16}$$

$$\mu_i=i\pi,\ i=1,2,3\cdots \tag{17}$$

The eigenfunctions satisfy the following orthonormal property:

$$\int_0^1X_i(\xi)X_j(\xi)\mathrm{d}\xi=\delta_{ij}=\begin{cases}1, & i=j\\ 0, & i\neq j\end{cases} \tag{18}$$

The integral transform and inverse pairs are defined by:

$$\bar{w}_i(\tau)=\int_0^1w(\xi,\tau)X_i(\xi)\mathrm{d}\xi \tag{19a}$$

$$w_i(\xi,\tau)=\sum_{i=1}^{\infty}X_i(\xi)\bar{w}_i(\tau) \tag{19b}$$

Multiplying the governing equation (Eq-11) by the eigenfunction $X_i(\xi)$ and integrating in $\xi\in[0,1]$, the gonvern equation can be rewritten:

$$\sum_{j=1}^{\infty}\left[L_{ij}\frac{\mathrm{d}^2\bar{w}_j(\tau)}{\mathrm{d}t^2}\right]+\sum_{j=1}^{\infty}\left[\alpha_o(A_{ij}^*\mu_j^4+C_{ij})+2U\sqrt{\beta}H_{ij}\right]\frac{\mathrm{d}\bar{w}_j(\tau)}{\mathrm{d}t}-2\alpha_oQ\sum_{j=1}^{\infty}\left[N_{ij}\bar{w}_j(\tau)\right]\sum_{j=1}^{\infty}\sum_{k=1}^{\infty}\left[G_{jk}\bar{w}_j(\tau)\frac{\mathrm{d}\bar{w}_k(\tau)}{\mathrm{d}t}\right]-Q\sum_{j=1}^{\infty}\left[F_{ij}\bar{w}_j(\tau)\right]\sum_{j=1}^{\infty}\sum_{k=1}^{\infty}\left[G_{jk}\bar{w}_j(\tau)\bar{w}_k(\tau)\right]+\sum_{j=1}^{\infty}\left[\left(A_{ij}\mu_j^4+B_{ij}+U^2D_{ij}+\sqrt{\beta}\dot{U}E_{ij}\right)\bar{w}_j(\tau)\right]=0 \tag{20}$$

where these coefficients defined by:

$$A_{ij} = \int_0^1 f(\xi) X_i X_j \mathrm{d}\xi \tag{21a}$$

$$A_{ij}^{*} = \int_0^1 h(\xi) X_i X_j \mathrm{d}\xi \tag{21b}$$

$$B_{ij} = 2\int_0^1 f'(\xi) X_i X_j''' \mathrm{d}\xi + \int_0^1 f''(\xi) X_i X_j'' \mathrm{d}\xi \tag{21c}$$

$$C_{ij} = 2\int_0^1 h'(\xi) X_i X_j''' \mathrm{d}\xi + \int_0^1 h''(\xi) X_i X_j'' \mathrm{d}\xi \tag{21d}$$

$$D_{ij} = \int_0^1 X_i X_j'' \mathrm{d}\xi \tag{21e}$$

$$E_{ij} = \int_0^1 (1-\xi) X_i X_j'' \mathrm{d}\xi \tag{21f}$$

$$G_{ij} = \int_0^1 X_i' X_j' \mathrm{d}\xi \tag{21g}$$

$$F_{ij} = \int_0^1 f(\xi) X_i X_j'' \mathrm{d}\xi + \int_0^1 f'(\xi) X_i X_j' \mathrm{d}\xi \tag{21h}$$

$$H_{ij} = \int_0^1 h'(\xi) X_i X_j' \mathrm{d}\xi \tag{21i}$$

$$N_{ij} = \int_0^1 h(\xi) X_i X_j'' \mathrm{d}\xi + \int_0^1 h'(\xi) X_i X_j' \mathrm{d}\xi \tag{21j}$$

$$L_{ij} = \int_0^1 \left[\beta + g(\xi)(1-\beta)\right] X_i X_j \mathrm{d}\xi \tag{21k}$$

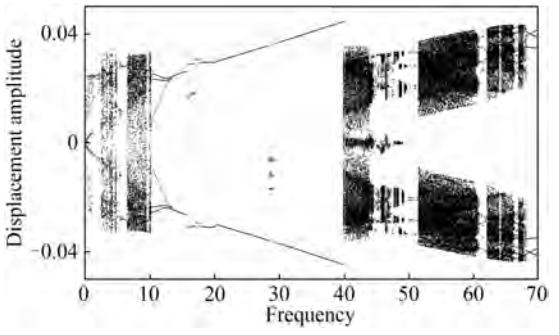

(a) Present study (*NW*=4)

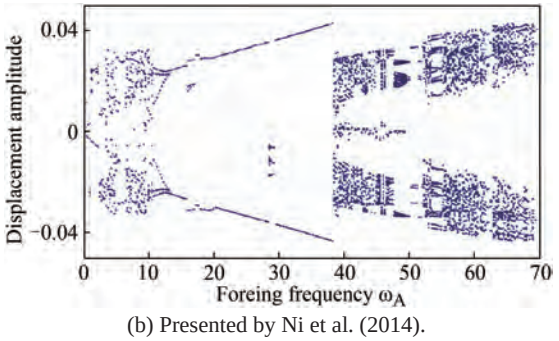

(b) Presented by Ni et al. (2014).

Figure 3 Bifurcation diagram of simply supported homogeneous pipe with $\beta = 0.6$, $U_0 = 4.5$, $\alpha_0 = 0.005$, $\psi = 0.4$, and $Q = 5\,000$

4 Results and discussion

4.1 Convergence analysis and results verification

As no previous study on nonlinear vibration results of the AFG pipe is encountered in the literature, the hybrid analytical-numerical solution is verified by analyzing the nonlinear vibration of the simply supported homogeneous pipe. Figure 3 shows the bifurcation diagram by the present study compared with that by Ni et al. (2014), for mass ratio $\beta = 0.6$, average flow velocity $U_0 = 4.5$, viscoelastic damping coefficient $\alpha_0 = 0.005$, pulsation amplitude $\psi = 0.4$, and slenderness ratio parameter $Q = 5\,000$. It can be seen that both the displacement amplitude and the bifurcation point are in good agreement with the results presented by Ni et al. (2014). It can be concluded that the proposed GITT solution for the nonlinear dynamics analysis of pipe was successfully verified.

Convergence analysis has been carried out to analyze the dynamic behavior of the simply supported AFG pipe under pulsating flow. Bifurcation diagrams of the transient displacement at the center of the pipe versus the dimensionless pulsation frequency are shown in Figure 4, with $\alpha_E = \alpha_{E^*} = \alpha_\rho = 2$, $\beta = 0.6$, $U_0 = 4.5$, $\alpha_0 = 0.005$, $\psi = 0.4$, and $Q = 5\,000$, calculated with NW= 2, 4, 6, and 8. As can be seen, when the dimensionless pulsation frequency of internal fluid is less than 40, there is no difference between the results with truncation orders *NW*=2, 4, 6 and 8. However, when the dimensionless pulsation frequency is greater than 40, there is the obvious difference between the bifurcation diagram with *NW*=2 and higher truncation orders (*NW*=4, 6 and 8). For truncation orders *NW*=4, 6, and 8, the variation of the bifurcation diagrams can be negleced. It can be concluded that the present hybrid numerical-analytical model (GITT mdoel) with *NW*=8 can predict the dynamic behavior of AFG pipes within the selected dimensionless frequency range $\omega \in [0,90]$. It can be seen from Figure 4 (d) that an AFG pipe ($k = 1$, $\alpha_E = \alpha_{E^*} = \alpha_\rho = 2$) has a complex dynamic behavior in the range of pulsation frequency from 0 to 90, presenting periodic, quasi-periodic, and even chaotic motions.

Figure 5 shows the phase portraits, Poincaré map, power spectra diagram, and time domain diagram for different dimensionless pulsation frequencies shown in Figure 4(d), which can reflect the characteristics of chaotic, quasi-periodic, and periodic motion. Within frequency range $\omega \in [0,10]$, the pipe shows aperiodic (chaotic) motion in a large frequency range, and the power spectra of chaotic motion show a broadband phenomenon without obvious main peaks, as shown by Figures 5 (a) and(b). There is also a small region of periodic motion, in the range of $\omega \in [5,6]$. In the range of $\omega \in [10,15]$, the chaotic motion becomes period-1 motion through the period-doubling bifurcation. From $\omega = 15$ to 36.7, the pipe vibration is mainly manifested as period-1 motion. The power spectrum of period-1 motion is a smooth curve with obvious main peaks, shown by Figure 5 (c), but there is a period-doubling motion near $\omega = 16$. For $\omega \in [36.7,52.6]$, the periodic motion is

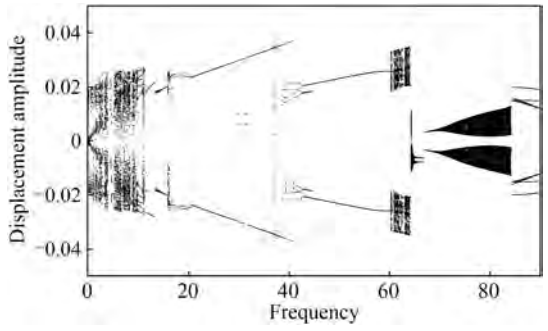

(a) NW=2

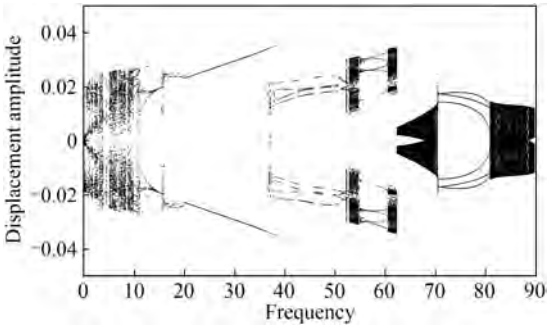

(b) NW=4

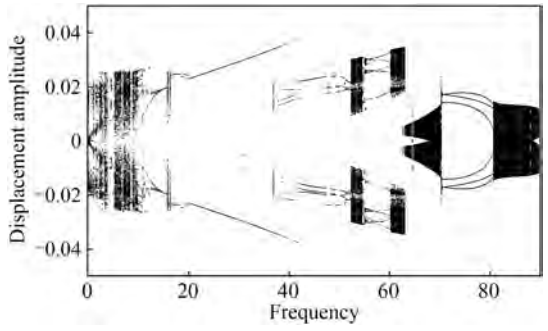

(c) NW=6

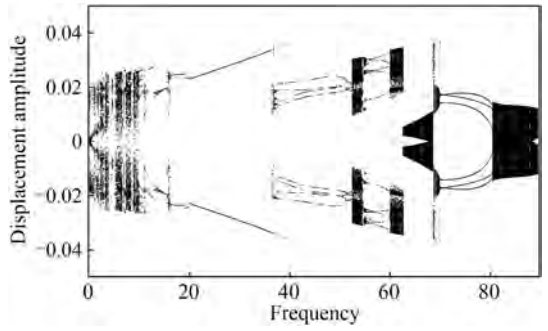

(d) NW=8

Figure 4 Convergence study of bifurcation diagram of AFG pipe with different truncated number (NW) when β = 0.6, U_0 = 4.5, α_E = α_{E^*} = α_ρ = 2, α_0 = 0.005, ψ = 0.4, and Q = 5 000

observed. For $\omega \in [52.6,54.7]$ and $[60.8,63.6]$, the AFG pipe is mainly manifested as chaotic motion, but between the two ranges, periodic motion is observed. In the range of $\omega \in [63.6,90]$, except for period-3 motion in $\omega \in [70.2,80.7]$, all the other frequencies induce quasic-periodic motion.

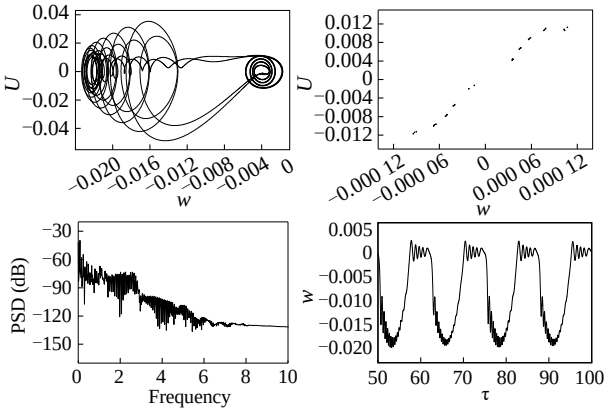

(a) ω=0.5, chaotic motion

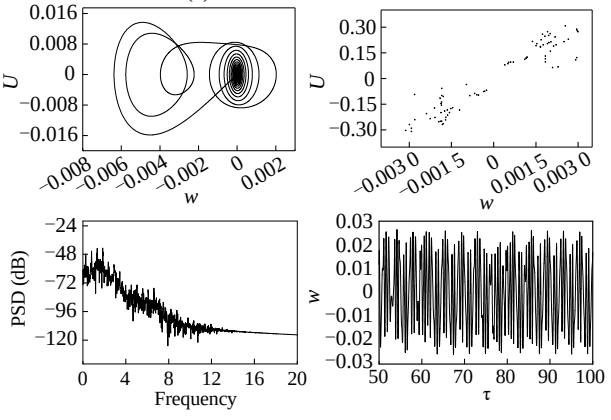

(b) ω=10, chaotic motion

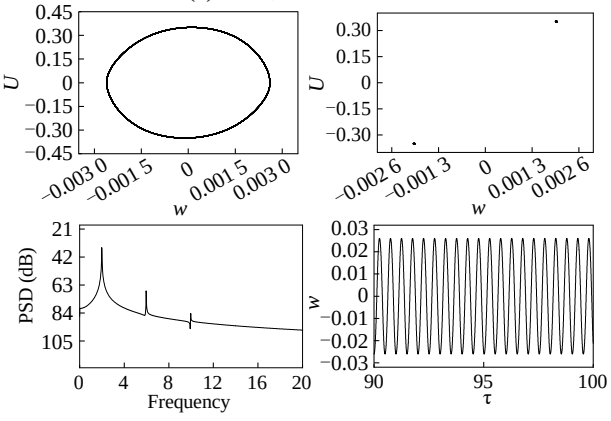

(c) ω=25, period-1 motion

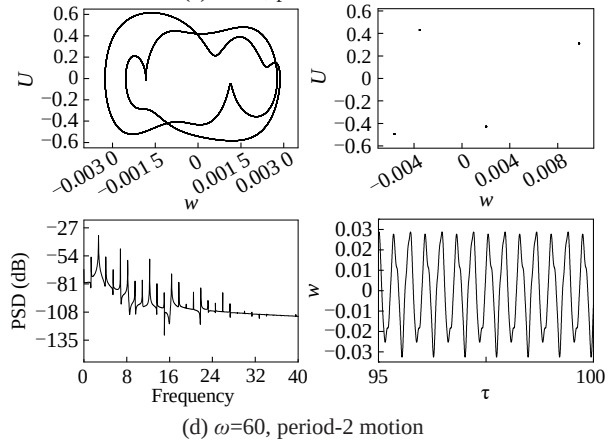

(d) ω=60, period-2 motion

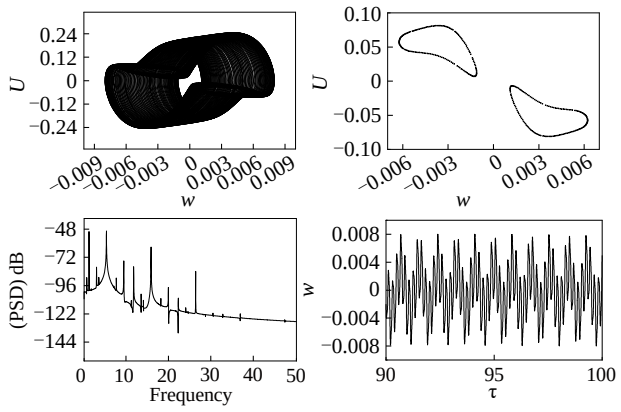

(e) ω=66, quasi-periodic motion

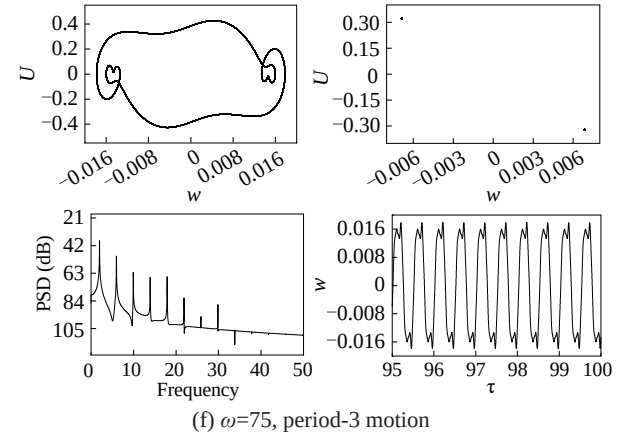

(f) ω=75, period-3 motion

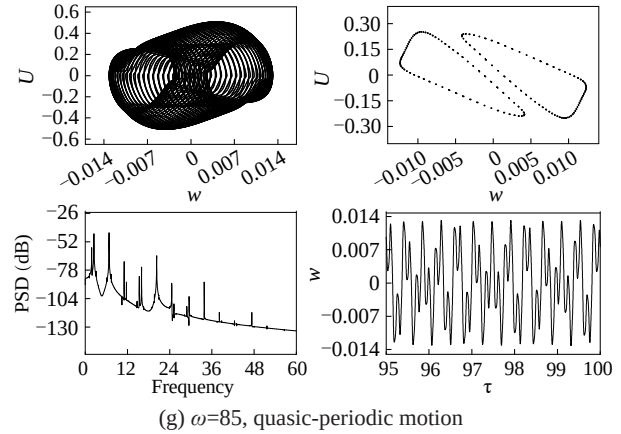

(g) ω=85, quasic-periodic motion

Figure 5 Phase portraits diagram, Poincaré diagram, power spectra, and time-domain phase diagram at the midpoint under different pulsation frequencie

The power spectrogram of quasic-periodic motion has a wide frequency phenomenon at the same time and an obvious main peak is shown in Figure 5e.

4.2 Influence of elastic modulus distribution on system dynamic behavior

Figures 6–8 show the parametric analysis of the elastic modulus distribution on the dynamic response of the AFG pipe, with the homogeneous density and coefficient of viscoelastic damping ($\alpha_{E^*} = \alpha_\rho = 1$). The elastic modulus ratio α_E is taked as 2, and k is takend as 0.1, 0.5, 1, 2, 5 and 10.

Figure 6 (a) shows the bifurcation diagram of AFG pipe with k=0.1. In the range of $\omega \in [0,11.7]$, the pipe is mainly manifested as chaotic motion, and there are also areas of

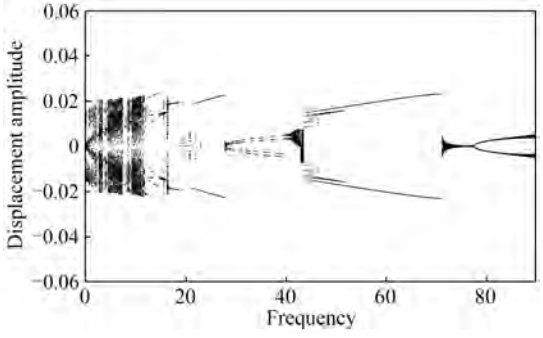

(a) k=0.1

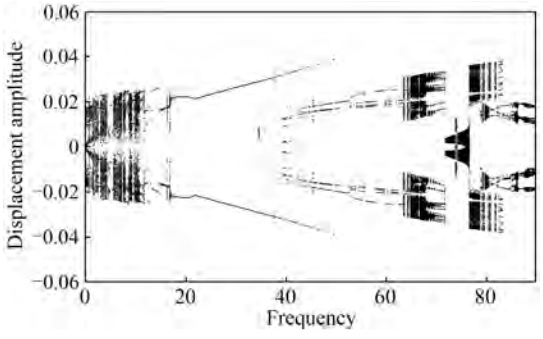

(b) k=0.5

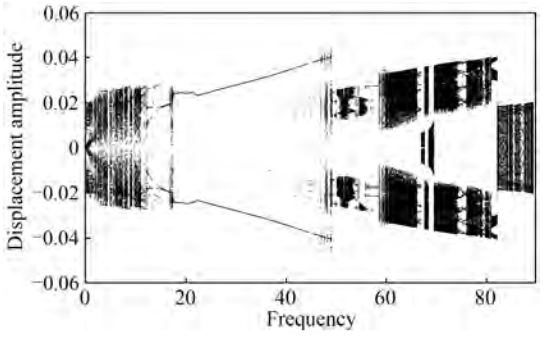

(c) k=1.0

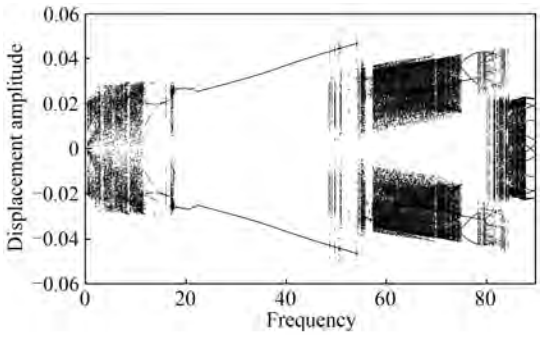

(d) k=2.0

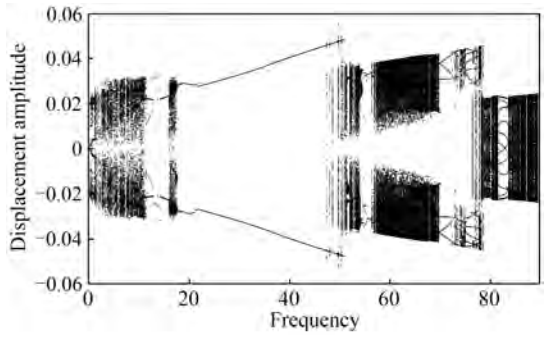

(e) k=2.0

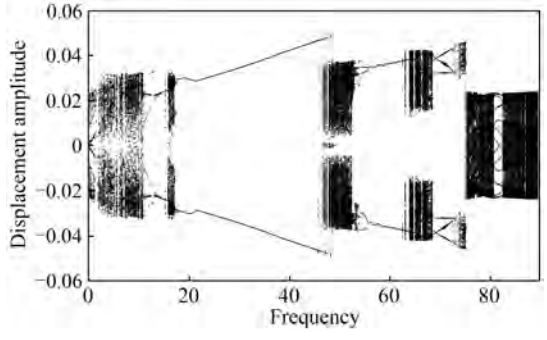

(f) k=10.0

Figure 6 Influence of the distribution of elastic modulus on the dynamic behavior of AFG pipe

partial periodic motion, for instance $\omega \in [7.5,8]$. In the range of $\omega \in [11.7,15]$, chaotic motion is changed into period-1 motion. In the range of $\omega \in [15,28]$, periodic motion is mainly observed. From ω = 28 to 41.5, it is manifested as period-1 motion. In the range of $\omega \in [42.6,70]$, it is mainly manifested as multi-period motion. From the range of ω= 70 to 90, the static equilibrium state is transformed into periodic motion through Hopf bifurcation. Figure 6(b) shows the bifurcation diagram for k = 0.5. For dimensionless frequency ω=0 to 11.7, it is mainly manifested as chaotic motion, and there is also periodic motion, such as in the range of $\omega \in [5,5.5]$. Within the range of $\omega \in [11.7,63.5]$, it is mainly manifested as periodic ω = 10, 50, 60, and 70 motion. For dimensionless pulsation frequency ω =63.6 to 72, chaotic motion is transformed into periodic motion. For dimensionless frequency ω=72 to 76.8, it is mainly manifested as quasi-periodic motion. In the frequency range of $\omega \in [76.85,90]$, chaotic motion is transformed into periodic motion. For k = 1, as shown in Figure 6 (c), in the range of $\omega \in [45.5,82]$, there exists a large range of chaotic motion, as well as a small range of periodic motion ($\omega \in [75,76.3]$) and quasi-periodic motion ($\omega \in [68.8,69.8]$). Within the range of $\omega \in [82,90]$, the motion is quasi-periodic. As seen in Figure 6 (c)–(f), when $k \geqslant 1$the motion state in the low-frequency region ($\omega \in [0,45.5]$) is stable and does not change with changing k, while there is a large difference in the high-frequency region. With increasing k, the chaotic region in the high frequency region $\omega \in [45.5,90]$

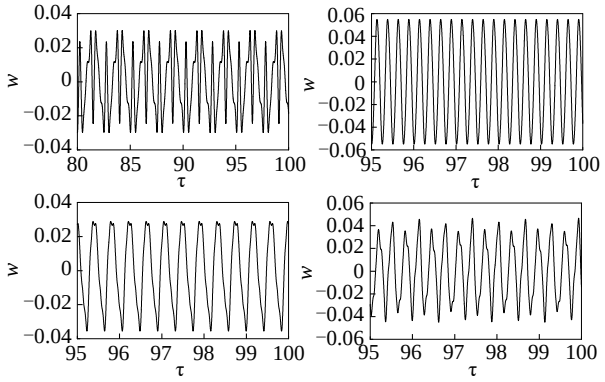

(a) k=0.5

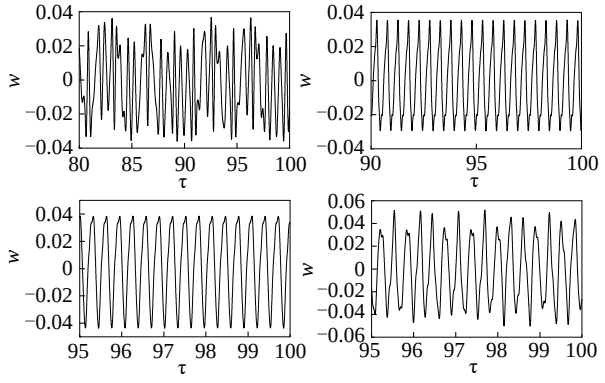

(b) k=1.0

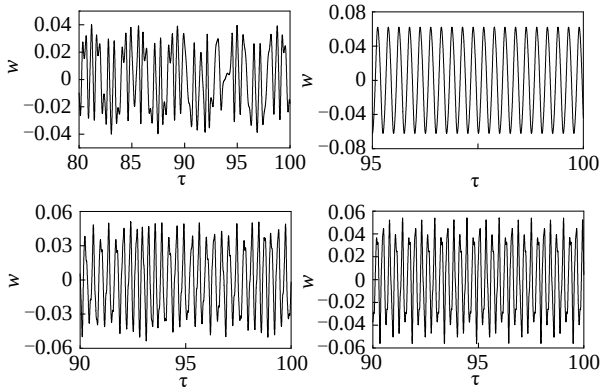

(c) k=2.0

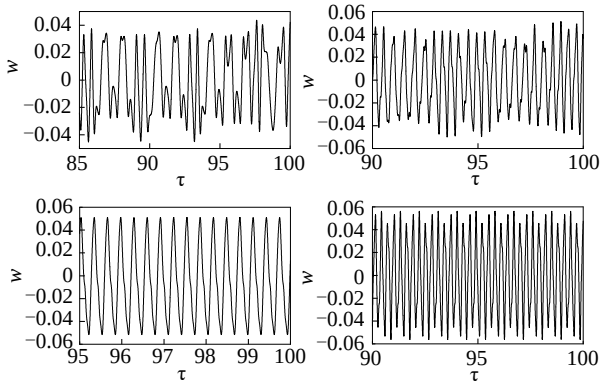

(d) k=10.0

Figure 7 Time domain diagram of the system at different k and pulsation frequencies when ω = 10, 50, 60, and 70 , repectively

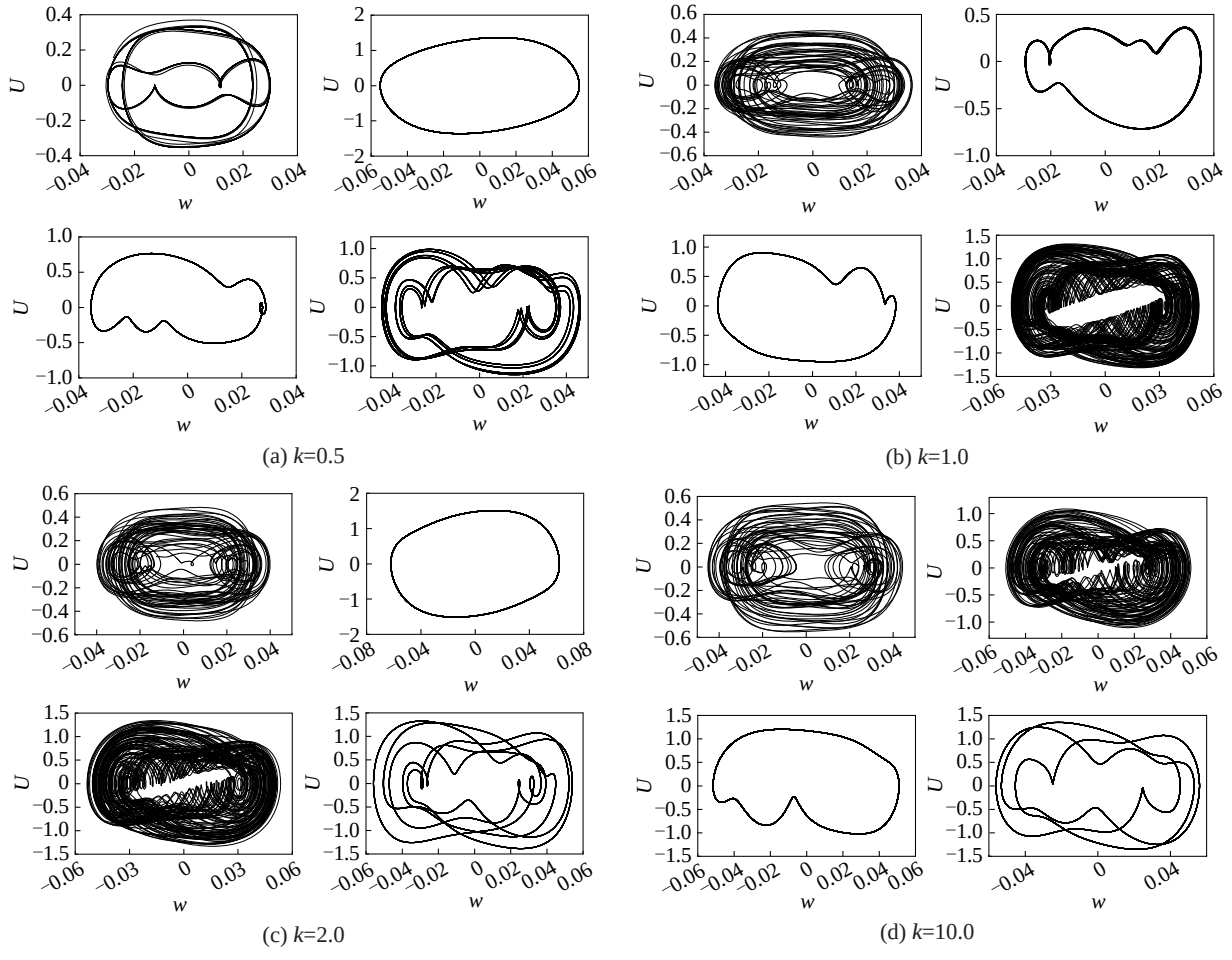

(a) k=0.5 (b) k=1.0

(c) k=2.0 (d) k=10.0

Figure 8 Phase portraits of the system at different k and pulsation frequencies when ω = 10, 50, 60, and 70 **,** repectively

is squeezed, while the periodic and quasi-periodic regions will be extended.

4.3 Influence of distribution coefficients of viscoelastic damping and density on the system dynamic behavior

It is assumed that the density and elastic modulus of the functionally gradient material pipe are uniform in all directions ($\alpha_E = \alpha_\rho = 1$), the coefficient of viscoelastic damping ratio $\alpha_{E^*} = 2$, and k is taken as 0.1, 0.5, 1, 2, 5, and 10 to analyze the influence of the coefficient of viscoelastic distribution on the dynamic response of AFG pipes.

As shown in Figures 9 (a) and (b), when $k < 1$, the bifurcation diagram of dimensionless pulsation frequency changes little in the range of $\omega \in [0,90]$, and there are great differences mainly in the range of frequency $\omega \in [67,76]$. When $k = 0.1$, it shows period-1 motion, and there is also a small range of period-3 motion, as shown in Figure 9 (a). When $k = 0.5$, period-3 motion is transformed into period-1 motion, as shown in Figure 9 (b). When $k = 1$, the motion is transformed from multi-periodic motion to period-1 motion, as shown in Figure 9 (c). When $k > 1$, the region with great variation in the bifurcation diagram is within the range of frequency $\omega \in [50,60]$ and $\omega \in [70,90]$. Within $\omega \in [50,60]$, when $k = 2$, it mainly manifests as multi-periodic motion. When $k = 5$ and $k = 10$, chaotic motion is mainly manifested in a larger range. When the dimensionless frequency increases from ω=70 to 90, the range of quasi-periodic motion will increase gradually with increasing k. It can be seen that the k has a great influence on the motion state at high frequency, and its influence on the motion state at low frequency can be neglected.

It is assumed that the elastic modulus and coefficient of viscoelastic damping of AFG pipe are nonuniform ($\alpha_E = \alpha_{E^*} = 1$), the density ratio $\alpha_\rho = 2$, and k is taken as 0.1, 0.5, 1, 2, 5, and 10 to analyze the influence of density distribution on the dynamic response of the pipe. Figure 10 (a) shows the bifurcation diagram for AFG pipe with $k = 0.1$. In the range of $\omega \in [0,10]$, the pipe is in chaotic motion, but there are also a few pulsation frequencies such as $\omega \in [4.5,6]$ that are in periodic motion. Within frequency range $\omega \in [9.6,11.6]$, it appears as period-3 motion. When the frequencyωincreases from 11.6 to 34.4, the period-1

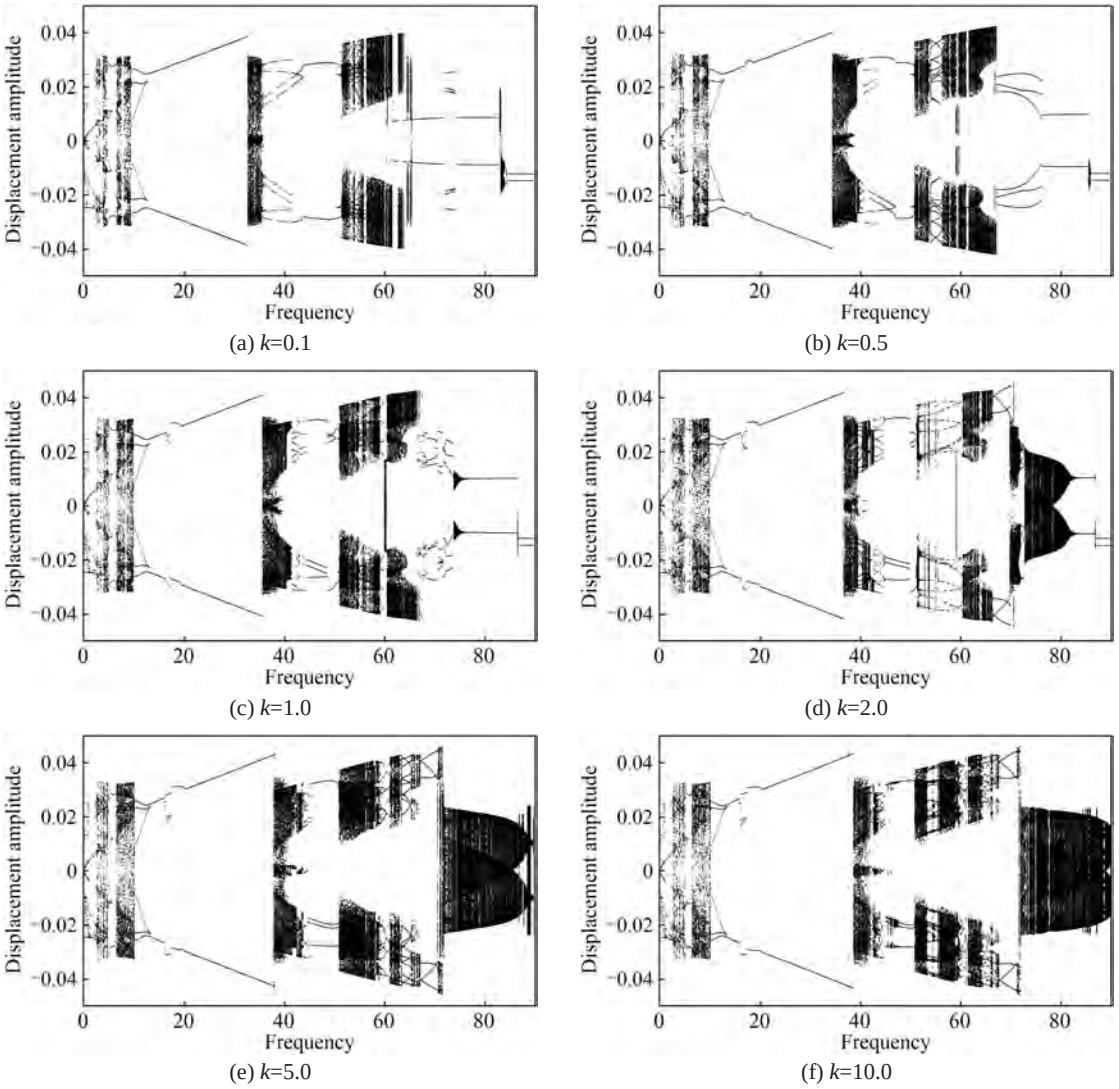

(a) k=0.1 (b) k=0.5

(c) k=1.0 (d) k=2.0

(e) k=5.0 (f) k=10.0

Figure 9 Influence of the coefficient of viscoelastic damping distribution on the dynamic behavior of AFG pipe

motion appears, but a sudden change occurs at the dimensionless pulsation frequency of 12.6, changing from period-1 motion to period-2 motion and lasting to the frequency of 13.6. In the range of $\omega \in [34.4,61.5]$, it is mainly manifested as chaotic motion, but periodic motion and quasi-periodic motion can also be observed. Within frequency range $\omega \in [61.5,90]$, it is mainly manifested as quasi-periodic motion, and there is also a small range of periodic motion.

It can be seen from Figure 10 that when the dimensionless pulsation frequency ω is less than 34.4, the effects of the material variation index k on the dynamic response of AFG pipes can be ignored. However, when $\omega > 34.4$, with increasing k, the frequency range of period-1 motion will gradually extended, and the chaotic and quasi-periodic motion frequency regions will not be changed, but the frequency of chaotic and quasi-periodic motion will gradually increase. Therefore, it can be concluded that the k has almost no effect on the motion state under low frequency range ($\omega \in [0,34.4]$). However, in the high frequency region, with increasing k, the motion state will not change, but the starting frequency at which each motion state occurs is increased.

5 Conclusion

The nonlinear dynamics of AFG pipe conveying pulsating flow is studied by using the generalized integral transform technique. The effects of the elastic modulus, density and coefficient of viscoelastic damping distribution on the dynamic behavior of the pipe are investigated, with the following main conclusions.

The distribution of the elastic modulus has an important influence on the motion state of the system. When the index of material variation $k < 1$, it has a greater influence on the motion in both low-frequency and high-frequency regions. However, when $k > 1$, it has a greater effect on

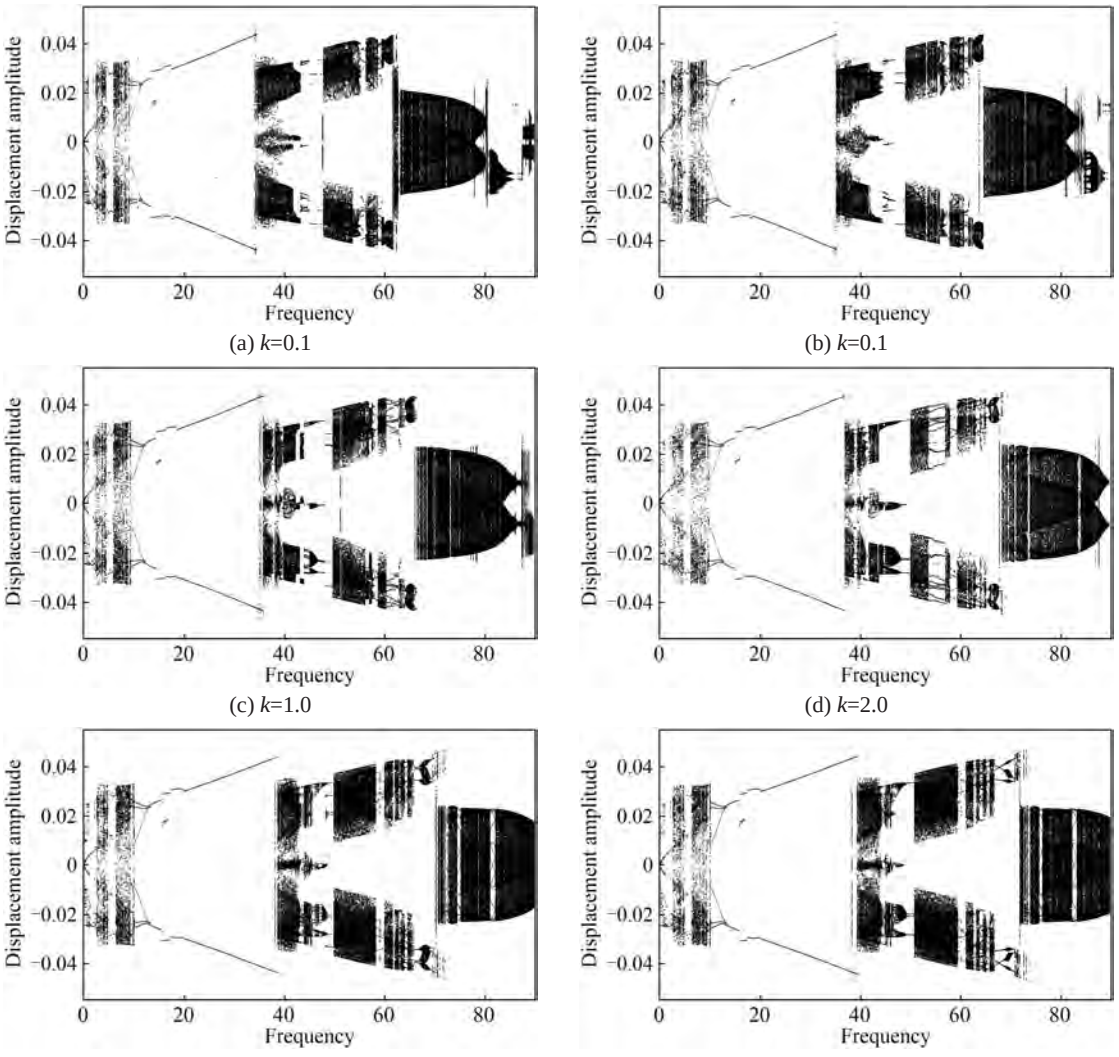

(a) k=0.1 (b) k=0.1

(c) k=1.0 (d) k=2.0

(e) k=5.0 (f) k=10.0

Figure 10 Influence of density distribution on the dynamic behavior of AFG pipe

the motion only at high frequencies, with negligible effects in the low frequency region.

The distribution of density has little effect on the motion state of the system, with k having a great influence on the motion state at high frequency, but almost no influence on the motion state at low frequency.

The distribution of the viscoelastic damping coefficient has an important effect on the motion state of the system. In the low frequency region, the k has almost no effect on the motion state. With the increase in k, the motion state at high frequency region will not change, but the starting frequency at which each motion state occurs is increased.

The present method can be extended to the analysis of on nonlinear dynamics of viscoelastic AFG pipe conveying pulsating fluid with other classical boundary conditions, such as clamped and free ends, or more general elastic boundary conditions such as rotationally restrained ends. It can also be extended to the analysis of linear and nonlinear stability of mooring cables or catenary risers using large-deflection Euler-Bernoulli beam models.

Funding This work is supported by the National Natural Science Foundation of China (52171288, 51890914), the Key Research and Development Program of Shandong Province (Major Innovation Project) (2022CXGC020405), the National Ministry of Industry and Information Technology Innovation Special Project—Engineering Demonstration Application of Subsea Oil and Gas Production System-Subject 4 “Research on Subsea Christmas Tree and Wellhead Offshore Testing Technology” [MC-201901-S01-04], the Fundamental Research Funds for the Central Universities (20CX02410A), the Development Fund of Shandong Key Laboratory of Oil & Gas Storage and Transportation Safety, and CNPq, CAPES and FAPERJ of Brazil.

Competing interest The authors have no competing interests to declare that are relevant to the content of this article.

References

An C, Su J (2017) Dynamic behavior of axially functionally graded

pipes conveying fluid. Mathematical Problems in Engineering 2017: 6789634. https://doi.org/10.1155/2017/6789634

Babilio E (2014) Dynamics of functionally graded beams on viscoelastic foundation, International Journal of Structural Stability and Dynamics 14 (08): 1440014. https://doi.org/10.1142/S0219455414400148

Cotta RM, Lisboa KM, Curi MF, Balabani S, Quaresma JN, Perez Guerrero JS, Macˆedo EN, Amorim NS (2019) A review of hybrid integral transform solutions in fluid flow problems with heat or mass transfer and under Navier – Stokes equations formulation. Numerical Heat Transfer, Part B: Fundamentals 76 (2): 60–87. https://doi.org/10.1080/10407790.2019.1642715

Dai J, Liu Y, Liu H, Miao C, Tong G (2019) A parametric study on thermo-mechanical vibration of axially functionally graded material pipe conveying fluid. International Journal of Mechanics and Materials in Design 15 (4): 715–726. https://doi.org/ 10.1007/s10999-018-09439-5

Deng J, Liu Y, Zhang Z, Liu W (2017) Dynamic behaviors of multi-span viscoelastic functionally graded material pipe conveying fluid. Proceedings of the Institution of Mechanical Engineers, Part C: Journal of Mechanical Engineering Science 231 (17): 3181-3192. https://doi.org/10.1177/0954406216642483

Ebrahimi-Mamaghani A, Sotudeh-Gharebagh R, Zarghami R, Mostoufi N (2022) Thermo-mechanical stability of axially graded rayleigh pipes. Mechanics Based Design of Structures and Machines 50(2): 412-441. https://doi.org/10.1080/15397734.2020.1717967

Fu G, Li M, Yang J, Li S, Sun B, Estefen S F (2022a) A simplified equation for the collapse pressure of sandwich pipes with different core materials. Ocean Engineering 254: 111292. https://doi. org/10.1016/j.oceaneng.2022.111292

Fu G, Li M, Yang J, Sun B, Shi C, Estefen S F (2022b) The effect of eccentricity on the collapse behaviour of sandwich pipes. Applied Ocean Research 124(4): 103190. https://doi.org/10.1016/j.apor.2022.103190

Fu G, Peng Y, Sun B, An C, Su J (2019) An exact GITT solution for static bending of clamped parallelogram plate resting on an elastic foundation. Engineering Computations 36 (6): 2034–2047. https://doi.org/10.1108/EC-12-2018-0582

Fu G, Tuo Y, Sun B, Shi C, Su J (2022c) Bending of variable thickness rectangular thin plates resting on a double-parameter foundation: integral transform solution. Engineering Computations 39 (7): 2689–2704. https://doi.org/10.1108/EC-11-2021-0692

Gupta A, Talha M (2015) Recent development in modeling and analysis of functionally graded materials and structures. Progress in Aerospace Sciences 79:1–14. https://doi.org/10.1016/j.paerosci.2015.07.001i

Heshmati M (2020) Influence of an eccentricity imperfection on the stability and vibration behavior of fluid-conveying functionally graded pipes. Ocean Engineering 203: 107192. https://doi. org/10.1016/j.oceaneng.2020.107192

Jiang M, Zhao J, Wang Q (2022) Linear energy stable numerical schemes for a general chemo-repulsive model. Journal of Computational and Applied Mathematics, 114436. https://doi.org/10.1016/j.cam.2022.114436

Jiang M, Zhao J (2023) Linear relaxation schemes for the Allen-Cahn-type and Cahn-Hilliard-type phase field models. Applied Mathematics Letter 137: 108477. https://doi.org/10.1016/j.aml.2022.108477

Jin JD (1997) Stability and chaotic motions of a restrained pipe conveying fluid. Journal of Sound and Vibration 208 (3): 427–439. https://doi.org/10.1006/jsvi.1997.1195

Jin J, Song Z (2005) Parametric resonances of supported pipes conveying pulsating fluid. Journal of Fluids and Structures 20 (6): 763–783. https://doi.org/10.1016/j.jfluidstructs.2005.04.007

Khodabakhsh R, Saidi A R, Bahaadini R (2020) An analytical solution for nonlinear vibration and post-buckling of functionally graded pipes conveying fluid considering the rotary inertia and shear deformation effects. Applied Ocean Research 101: 102277. https://doi.org/10.1016/j.apor.2020.102277

Li F, An C, Duan M, Su J (2020) Combined damping model for dynamics and stability of a pipe conveying two-phase flow. Ocean Engineering 195: 106683. https://doi.org/10.1016/j.oceaneng.2019.106683

Loghman E, Kamali A, Bakhtiari-Nejad F, Abbaszadeh M (2021) Nonlinear free and forced vibrations of fractional modeled viscoelastic FGM micro-beam, Applied Mathematical Modelling 92: 297–314. https://doi.org/10.1016/j.apm.2020.11.011

Lu Z Q, Zhang K K, Ding H, Chen L Q (2020) Nonlinear vibration effects on the fatigue life of fluid-conveying pipes composed of axially functionally graded materials. Nonlinear Dynamics 100 (2):1091–1104. https://doi.org/ 10.1007/s11071-020-05577-8

Ni Q, Zhang Z, Wang L, Qian Q, Tang M (2014) Nonlinear dynamics and synchronization of two coupled pipes conveying pulsating fluid. Acta Mechanica Solida Sinic 27 (2): 162 – 171. https://doi.org/ 10.1016/S0894-9166(14)60026-4

Nikbakht S, Kamarian S, Shakeri M (2019) A review on optimization of composite structures part ii: Functionally graded materials. Composite Structures 214: 83-102. https://doi. org/ 10.1016/j.compstruct.2019.01.105

Oyelade AO, Oyediran A A (2020) The effect of various boundary conditions on the nonlinear dynamics of slightly curved pipes under thermal loading. Applied Mathematical Modelling 87: 332–350. https://doi.org/10.1016/j.apm.2020.06.019

Paidoussis M (1987) Flow-induced instabilities of cylindrical structures 40(2): 163-175. https://doi.org/ 10.1115/1.3149530

Paidoussis M, Cusumano J, Copeland G (1992) Low-dimensional chaos in a flexible tube conveying fluid. Journal of Applied Mechanics 59(1):196–205. https://doi.org/10.1115/1.2899428

Paidoussis M, Issid N (1974) Dynamic stability of pipes conveying fluid. Journal of Sound and Vibration 33 (3): 267–294. https://doi.org/ 10.1016/S0022-460X(74)80002-7

Paidoussis M, Li G, Moon F (1989) Chaotic oscillations of the autonomous system of a constrained pipe conveying fluid. Journal of Sound and Vibration 135(1): 1-19. https://doi. org/ 10.1016/0022-460X(89)90750-5

Paıdoussis M, Li G (1993) Pipes conveying fluid: a model dynamical problem, Journal of Fluids and Structures 7(2): 137-204. https://doi.org/ 10.1006/jfls.1993.1011

Paidoussis M, Moon F (1988) Nonlinear and chaotic fluid elastic vibrations of a flexible pipe conveying fluid, Journal of Fluids and Structures 2(6): 567-591. https://doi.org/10.1016/S0889-9746(88)80023-9

Paidoussis M, Semler C (1993) Nonlinear and chaotic oscillations of a constrained cantilevered pipe conveying fluid: a full nonlinear analysis. Nonlinear Dynamics 4 (6): 655-670. https://doi. org/ 10.1007/BF00162236

Shafiei N, She G L (2018) On vibration of functionally graded nano-tubes in the thermal environment. International Journal of Engineering Science 133: 84-98. https://doi.org/10.1016/j.ijengsci.2018.08.004

Shariati A, Mohammad-Sedighi H, Zur K K, Habibi M, Safa M (2020) On the vibrations and stability of moving viscoelastic axially functionally graded nanobeams. Materials 13 (7): 1707. https://doi.org/ 10.3390/ma13071707

Shen J, Xu J, Yang J (2018) The scalar auxiliary variable (SAV)

approach for gradient flows. Journal of Computational Physics 353:407-416. https://doi.org/10.1016/j.jcp.2017.10.021

Tang D, Dowell E (1988) Chaotic oscillations of a cantilevered pipe conveying fluid. Journal of Fluids and Structures 2 (3): 263-283. https://doi.org/ 10.1016/S0889-9746(88)80011-2

Tang Y, Yang T (2018) Post-buckling behavior and nonlinear vibration analysis of a fluid conveying pipe composed of functionally graded material. Composite Structures 185: 393-400. https://doi.org/ 10.1016/j.compstruct.2017.11.032

Tuo Y, Fu G, Sun B, Lou M, Su J (2022) Stability of axially functionally graded pipe conveying fluid: Generalized integral transform solution. Applied Ocean Research 125:103218. https://doi.org/ 10.1016/j.apor.2022.103218

Wang L (2009) A further study on the non-linear dynamics of simply supported pipes conveying pulsating fluid. International Journal of Non-Linear Mechanics 44 (1): 115-121. https://doi.org/ 10.1016/j.ijnonlinmec.2008.08.010

Wang L, Liu Z, Abdelkefi A, Wang Y, Dai H (2017) Nonlinear dynamics of cantilevered pipes conveying fluid: towards a further understanding of the effect of loose constraints, International Journal of Non-Linear Mecha 95: 19-29. https://doi.org/ 10.1016/j.ijnonlinmec.2017.05.012

Wang Y, Chen Y (2019) Dynamic analysis of the viscoelastic pipeline conveying fluid with an improved variable fractional order model based on shifted Legendre polynomials. Fractal and Fractional 3 (4): 52. https://doi.org/10.3390/fractalfract3040052

Wang Z, Soares C G (2021) Upheaval thermal buckling of functionally graded subsea pipelines. Applied Ocean Research 116: 102881. https://doi.org/ 10.1016/j.apor.2021.102881

Wang Z, Chen B, Soares CG (2022) Analytical study on the upheaval thermal buckling of sandwich pipes. Marine Structures 85: 103245. https://doi.org/10.1016/j.marstruc.2022.103245

Zhao J, Wang Q, Yang X (2017) Numerical approximations for a phase field dendritic crystal growth model based on the invariant energy quadratization approach. International Journal for Numerical Methods in Engineering 110: 279-300. https://doi.org/10.1002/nme.5372

Zhou X W, Dai H L, Wang L (2018) Dynamics of axially functionally graded cantilevered pipes conveying fluid. Composite Structures 190: 112-118. https://doi.org/10.1016/j.compstruct.2018.01.097